Surface Science Hot Paper

International Edition: DOI: 10.1002/anie.201909593
German Edition: DOI: 10.1002/ange.201909593

Long-Range Chirality Recognition of a Polar Molecule on Au(111)

Huihui Kong, Yinyue Qian, Xinbang Liu, Xinling Wan, Saeed Amirjalayer, and Harald Fuchs**

Abstract: *Chiral molecular self-assemblies were usually achieved using short-range intermolecular interactions, such as hydrogen-, metal–organic, and covalent bonding. However, unavoidable surface defects, such as step edges, surface reconstructions, or site dislocations may limit the applicability of short-range chirality recognition. Long-range chirality recognition on surfaces would be an appealing but challenging strategy for chiral reservation across surface defects at long distances. Now, long-range chirality recognition is presented between neighboring 3-bromo-naphthalen-2-ol (BNOL) stripes on an inert Au(111) surface across the herringbone reconstruction as investigated by STM and DFT calculations. The key to achieving such recognition is the herringbone reconstruction-induced local dipole accumulation at the edges of the BNOL stripes. The neighboring stripes are then forced to adopt the same chirality to create the opposite edged dipoles and neutralize the neighbored dipole moments.*

The advanced fabrication of desired chiral nanostructures on solid surfaces has recently received tremendous interest owing to their potential applications in enantioselective heterogeneous catalysis,[1–3] non-linear optical devices,[4] chiral separations, and enantiospecific sensors.[5] Understanding how molecular chirality is recognized, transferred, and amplified at surfaces is a mandatory basis for artificial modulation of chiral behavior, chirality separation and further precise construction of homochiral architectures. Scanning tunneling microscopy (STM) has been demonstrated to be able to directly reveal molecular and supramolecular chirality and give unprecedented insights in unraveling the underlying formation mechanism for the chiral nanostructures on surfaces.[6–8] It has been demonstrated that chirality recognition is generally achieved through short-range intermolecular attractive interactions, such as C–H···π interaction,[9–10] hydrogen bonding,[11–15] metal–organic coordination,[16–20] and covalent bonding.[6,21–22] Such intermolecular short-range chirality recognition represents common routes to facilitate selective aggregation of homochiral molecule into chiral self-assembled nanostructures. However, it should be noted that defects on surfaces, such as step edges, surface reconstructions, or site dislocations often exist and are almost unavoidable, and these defects may limit the short-range chirality recognition in these regions. It is therefore of great interest to study the possibility of chirality recognition across long distance, especially across the surface reconstruction which is a frequent phenomenon on metal surfaces. Such an investigation may shed light on chirality recognition in long range and further facilitate the fabrication of sophisticated nanoarchitectures with specific chirality across potential defects.

To study the chirality recognition over longer ranges, the strategy herein is first to select an appropriate substrate with corrugations that could effectively separate the chiral molecules or aggregations from each other. For such studies, Au(111) provides an ideal model system as the herringbone reconstruction is found to separate the Au(111) into several remarkably varying adsorption potential region for organic molecules, including FCC-, HCP-, and bridge regions.[23–25] We have selected the 3-bromo-naphthalen-2-ol (BNOL) molecule as BNOL is prochiral, which makes it feasible for investigation of its chirality recognition behavior on Au(111). From the interplay of high-resolution STM imaging and DFT calculations, we have studied the chiral self-assembly of BNOL on Au(111) and the long-range chirality recognition process. We show that: 1) Deposition of BNOL molecules on Au(111) results in the formation of chiral trimer motifs by O–H···O and C–H···Br bonds; 2) the chiral trimer motifs can serve as elementary motifs and they connect with others by weaker C–H···Br bonds to self-assemble into chiral double or single-strand stripes (which are confined in FCC- or HCP-region) with a separation of about 1.0 nm; 3) interestingly, the neighbored stripes tend to adopt the same chirality, indicating the chirality recognition achieved across a remarkable distance of about 1.0 nm, which indicates a novel chirality preservation and replication over longer distances; and 4) the key to achieving such long-range chirality recognition is the herringbone reconstruction-induced accumulation of dipole moments at the edge of the chiral stripes. To create the opposite dipoles for neutralizing the dipoles at the edge of the neighbored stripes, the neighbored stripes are forced to adopt the same chirality, as revealed by density functional theory

[*] Dr. H. Kong, Y. Qian, X. Liu, X. Wan, Prof. Dr. H. Fuchs
Herbert Gleiter Institute of Nanoscience, School of Materials Science and Engineering, Nanjing University of Science and Technology
Nanjing 210094 (P. R. China)
E-mail: konghuihui@njust.edu.cn
fuchsh@uni-muenster.de
Dr. S. Amirjalayer, Prof. Dr. H. Fuchs
Physikalisches Institute, Westfälische Wilhelms-Universität Münster
Münster 48149 (Germany),
and
Center for Nanotechnology (CeNTech)
Heisenbergstrasse 11, 48149 Münster (Germany)
Dr. S. Amirjalayer
Center for Multiscale Theory and Computation (CMTC)
Heisenbergstrasse 11, 48149 Münster (Germany)
Supporting information and the ORCID identification number(s) for the author(s) of this article can be found under: https://doi.org/10.1002/anie.201909593.

(DFT) calculations. Such findings provide new avenue for the chirality recognition and help for design of novel chirality systems across defects in more complex systems.

Deposition of prochiral BNOL molecules on Au(111) leads to the formation of two sorts of chiral elementary structural motifs, that is, R- or L-chiral trimer, owing to the symmetry breakage induced by the Au(111) surface as depicted in Figure 1 a,b. Within such elementary structural motifs, each molecule exhibits the characteristic peanut configuration with a brighter protrusion at its head. After structural searches and comparison with high-resolution STM images, we have obtained two energetically most favorable mirrored configurations with the same energy (other energetically unfavorable gas-phase models are shown in the Supporting Information, Figure S1). Both of the DFT optimized models as well as the simulated STM images are found to correspond well with the experimental STM images as shown in Figure 1 c,d. From the optimized model in Figure 1 d, each chiral trimer is constructed by three homochiral BNOL molecules connecting with each other through O–H···O and C–H···Br hydrogen bonds. To study the chirality recognition behavior of such chiral trimers, the growth process has been demonstrated by the gradual increase of surface coverage step-by-step.

After deposition of BNOL molecules on Au(111) with coverage of about 0.5 monolayer (ML), the chiral BNOL trimers prefer to occupy the FCC region (see Figure 2 a,b). Such a situation is consistent with the phenomenon in previous reports[26,27] where the FCC region of the Au(111) reconstruction is considered to be energetically more favorable for adsorption of organic molecules. The fuzzy imaging at the HCP region may be induced by the swift diffusion of a few BNOL molecules. Well-ordered R- or L-chiral double-strand stripes with widths of around 3.8 nm are observed as shown in Figure 2 c,d. They grow along the direction (red arrows in Figure 2 a,b) rotated by 3.6° in clockwise or counterclockwise to the [11$\bar{2}$] direction (green arrow in Figure 2 a,b). Similarly as previously reported,[28] the growth of the double-strand stripes is influenced by the herringbone reconstruction. This is reflected by the definite growth direction (close to the herringbone reconstruction direction) rather than along the three equivalent directions of the three-fold symmetry of the Au(111) surface, as indicated in the Supporting Information, Figure S2. Close-up STM images further reveal that such

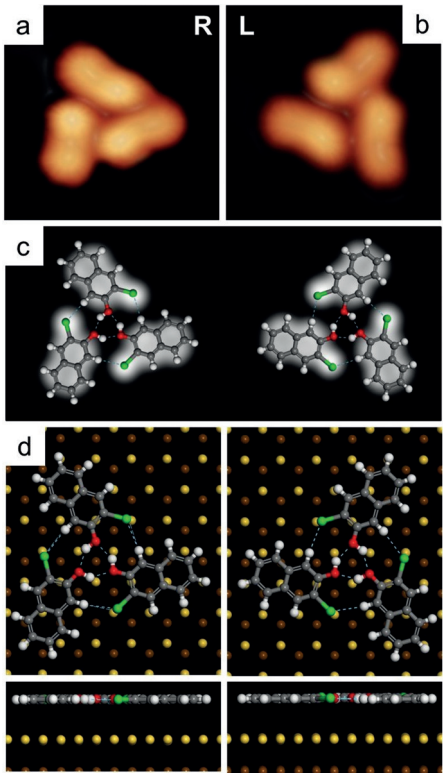

Figure 1. a),b) High-resolution STM images showing the R- and L-chiral trimers formed by BNOL molecules, respectively. c) Simulated STM images of R- and L-chiral trimers, overlaid by the DFT-optimized models. d) The corresponding top and side views of the models for R- and L-chiral trimers on Au(111). C gray, O red, H white, Br green, Au (top layer) yellow, Au (bottom layer) brown.

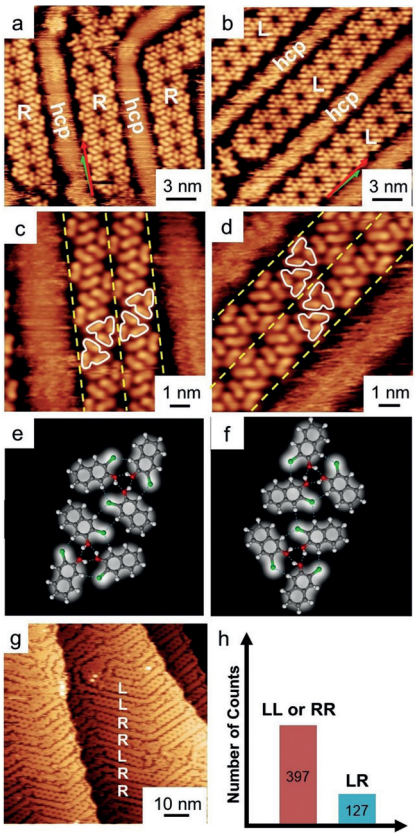

Figure 2. a),b) STM images showing the formation of R- and L-chiral double-strand stripes growing in the FCC region of Au(111). The red and green arrows indicate the direction of molecular stripes and the [11$\bar{2}$] direction of Au(111), respectively. c),d) Close-up STM images showing that R-and L-chiral double-strand stripes are formed by aggregation of R- and L-chiral trimer motifs, respectively. The yellow dashed line indicating the double-strand stripes formed by two stripes bound together, the white contours indicate the trimer motifs. e),f) Simulated STM images with the optimized models showing the chiral trimer motifs connecting with each other by double C–H···Br hydrogen bonds. g) Large-scale STM image showing the chirality of the double-strand stripes on the FCC region. h) Statistic histogram showing the chirality relationship of the adjacent double-strand stripes.

chiral double-strand stripes are constructed by the aggregation of trimer motifs with the same chirality as indicated by the white hand-drawing contours in Figure 2c and d. The optimized models together with the simulated STM image in Figure 2e,f demonstrate that C–H···Br hydrogen bonds serve as the driving force for the short-range chirality recognition in between the chiral trimers within the double-strand chiral stripes. From the model, the trimer motif could connect to another one (with the same chirality but anti-parallel orientation) from three distinct directions by equivalent C–H···Br bonds (Supporting Information, Figure S3a), which is also verified by the experimental results (Supporting Information, Figure S3b). However, the growth perpendicular across the herringbone reconstruction is inhibited, as indicated in the Supporting Information, Figure S3c. Thus, the formation of the observed double-strand stripes should be attributed to the confinement effect of the herringbone reconstruction. To study the long-range chirality recognition between the neighboring stripes in FCC region, we focused attention to large-scale STM image and performed statistical analysis. The STM image in Figure 2g shows that the neighbors of a L-chiral stripe could be either in L- or R-chiral forms. However, our statistical results reveal that the neighboring homochirality (LL + RR)/heterochirality (LR + RL) ratio is close to 3:1. This differs from the complete stochastic chirality distribution where a ratio of 1:1 (LL + RR/LR + RL) is expected. This indicates that the chirality behavior of the stripes in the FCC regions is influenced by their neighboring stripes (Figure 2h) to some extent with a separation of around 2.8 nm between neighbored double-strand stripes.

With the further increase of the surface coverage (ca. 0.8 ML), the growth of BNOL molecules starts to extend into HCP region of the Au(111) reconstruction and chiral single-strand stripes with a width of about 1.9 nm are formed in HCP region as shown in Figure 3a,b. The raised corrugation (that is, soliton walls) of the herringbone reconstruction separates the stripes in FCC and HCP region with a separation of about 1.0 nm (Supporting Information, Figure S4). High-resolution STM images (Figure 3c < ,dxfigr3 >) reveal that such single-strand chiral stripes are also formed by chiral trimer motifs connecting with each other by C–H···Br hydrogen bonds, as further verified by the good agreement of the experimental STM images with the simulated one based on the optimized model (Supporting Information, Figure S5). The limited latitude of HCP region should account for the single-strand stripes rather than double-strand ones in HCP region. Interestingly, by focusing on the chirality of neighbored stripes in Figure 3, we found that, compared to the chirality behavior between the double-strand stripes at lower coverage, the increased coverage (ca. 0.8 ML) leads to remarkable chirality recognition between adjacent stripes (Figure 3e). Such chirality recognition behavior is also supported by the statistical analysis on the chirality distribution of the stripes (Figure 3f). Furthermore, the full monolayer coverage leads to the formation of ordered chiral honeycomb nanostructures (Supporting Information, Figure S6).

Based on the above analysis, we consider that the chirality could be well preserved to its neighbors with a separation of about 1.0 nm (Supporting Information, Figure S4), which indicates a long-range chirality recognition. To provide theoretical evidence on such long-range chirality recognition between adjacent stripes, DFT-based calculations were performed. First, two models of chiral single-strand stripes with homochiral and heterochiral neighbors are built up in gas phase (Supporting Information, Figure S7). After relaxation, the calculations reveal an energy favor for homochiral stripes by a slight energy difference of 0.02 eV per unit cell. After including a two-layered Au(111) substrate (Supporting Information, Figure S8), such energy difference is tripled (that is, 0.06 eV), which is still relatively small. However, it should be noted that the chirality recognition is induced by the neighbored chiral stripes which often consist of more than 10 building blocks. Therefore, the energy difference for the whole stripes would be larger than 0.6 eV, which could greatly favor the neighbored stripes with the same chirality and rationalize the experimental long-range chirality recognition.

Then the question arises: what is the driving force for such long-range chirality recognition? As the separation between the neighbored stripes is around 1.0 nm (Supporting Information, Figure S4), which is much larger than the intermolecular distance for common chirality recognition through non-covalent attractive force (normally less than 0.4 nm). Also, we could rule out the substrate-induced repulsive force, which often works by the strong substrate-molecule interaction.[29] However, here we used a relatively inert Au(111) surface, which to our knowledge only exhibits strong interactions with thiol-contained molecules.[30,31]

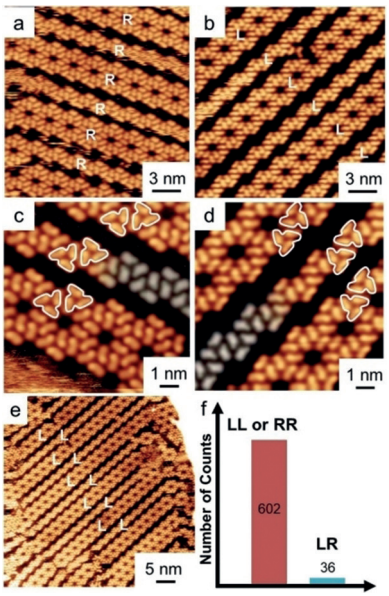

Figure 3. a),b) STM images showing that the increase of surface coverage further leads to the occupation of chiral single-strand stripes in the HCP region. c),d) Close-up STM images partially overlaid by the simulated STM image showing that the BNOL molecules within single-strand stripes connect together by the same mode and thus the same chiral nanostructure as double-strand ones despite of different latitude. e) Large-scale STM image showing the chirality of the double- and single-strand stripes on FCC and HCP region. f) Statistic histogram showing the chirality relationship of the adjacent stripes.

Careful examination on its chemical structure reveals that BNOL molecule should be considered as a polar molecule owing to the heterogeneous distribution of its function groups. Thus, the dipole accompanied with the image dipole would exist after adsorption of BNOL molecule on Au(111).[32] DFT calculations demonstrate that the dipole moment of single BNOL molecule is around 2.68 Debye along the direction indicated by the red arrow in Figure 4a. The dipole illustration (Figure 4b) reveals that most of the BNOL molecules appear in pairs with anti-parallel orientations which are close to each other (see the dashed green, pink, and yellow arrows in Figure 4b). Thus, the dipole moments of these paired molecules can compensate each other. However, net dipoles locally accumulate at the edge of both double and single-strand stripes (see red arrows in Figure 4b) owing to the herringbone reconstruction-confined growth of the BNOL molecule on Au(111).

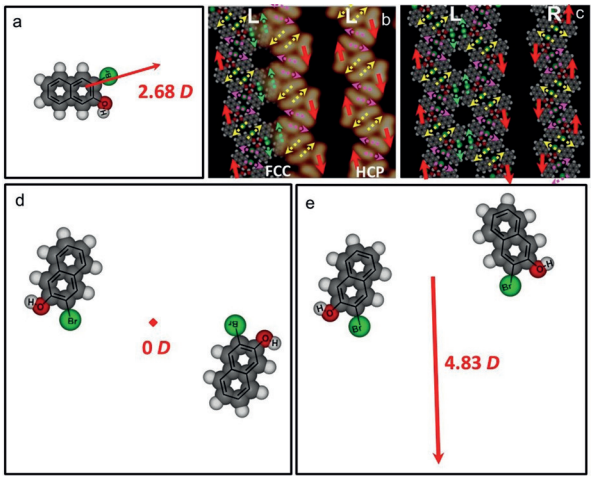

Figure 4. a) Dipole moment of single BNOL molecule. b),c) The dipole illustration of the neighbored stripes with homochirality (b) and heterochirality (c). The dashed dipoles indicate that two neighbored anti-parallel dipoles appear and generate no net dipole to the whole system. d) The two anti-parallel green dipoles almost generate no net dipole at the Bridge region. e) In contrast, the parallel green dipoles generate a net dipole of 4.83 D instead.

If the adjacent stripes adopt the same chirality (Figure 4b), then the nearest edged dipoles within these two stripes will adopt anti-parallel directions. The DFT calculations show that the two anti-parallel edged dipoles could compensate each other, and thus no net dipole is generated at the unoccupied region (see Figure 4d). Instead, for the heterogeneous chirality of the neighbored stripes (Figure 4c), there exist local net dipoles at the unoccupied region in between the stripes with a net dipole of around 4.83 Debye per unit cell (see Figure 4e), which would then lead to a large local dipole for the experimental stripes along the unoccupied region and make the whole system unstable. Therefore, to compensate the local edged dipoles, the neighbored stripes are forced to adopt the same chirality, which is considered to be the key to achieving the long-range chirality recognition on Au(111).

In conclusion, long-range chirality recognition between the BNOL stripes has been achieved on the Au(111) surface. The key to making the long-range chirality recognition feasible is the herringbone reconstruction-induced accumulation of dipoles at the edge of the stripes, which forces the neighbored stripes to adopt the same chirality to create opposite edged dipoles with the aim of neutralizing their neighbored dipole moments, as corroborated by DFT calculations.

Acknowledgements

The authors acknowledge financial support from the National Natural Science Foundation of China (21802072) and the Natural Science Foundation of Jiangsu Province (BK20170827).

Conflict of interest

The authors declare no conflict of interest.

Keywords: Au(111) · density functional calculations · dipoles · long-range chirality recognition · scanning tunneling microscopy

How to cite: *Angew. Chem. Int. Ed.* **2020**, *59*, 182–186
Angew. Chem. **2020**, *132*, 188–192

[1] M. Heitbaum, F. Glorius, I. Escher, *Angew. Chem. Int. Ed.* **2006**, *45*, 4732–4762; *Angew. Chem.* **2006**, *118*, 4850–4881.
[2] C. Baleizão, H. Garcia, *Chem. Rev.* **2006**, *106*, 3987–4043.
[3] H.-U. Blaser, *Tetrahedron: Asymmetry* **1991**, *2*, 843–866.
[4] V. Ostroverkhov, R. G. Petschek, K. D. Singer, R. J. Twieg, *Chem. Phys. Lett.* **2001**, *340*, 109–115.
[5] J. A. Switzer, H. M. Kothari, P. Poizot, S. Nakanishi, E. W. Bohannan, *Nature* **2003**, *425*, 490–493.
[6] H. Zhang, Z. Gong, K. Sun, R. Duan, P. Ji, L. Li, C. Li, K. Mullen, L. Chi, *J. Am. Chem. Soc.* **2016**, *138*, 11743–11748.
[7] S. Blankenburg, W. G. Schmidt, *Phys. Rev. Lett.* **2007**, *99*, 196107.
[8] Q. Chen, N. V. Richardson, *Nat. Mater.* **2003**, *2*, 324–328.
[9] M.-C. Blüm, E. Ćavar, M. Pivetta, F. Patthey, W.-D. Schneider, *Angew. Chem. Int. Ed.* **2005**, *44*, 5334–5337; *Angew. Chem.* **2005**, *117*, 5468–5471.
[10] L. Wang, H. Kong, X. Chen, X. L. Du, F. Chen, X. Q. Liu, H. M. Wang, *Appl. Phys. Lett.* **2009**, *95*, 093102.
[11] U. Schlickum, R. Decker, F. Klappenberger, G. Zoppellaro, S. Klyatskaya, W. Auwarter, S. Neppl, K. Kern, H. Brune, M. Ruben, J. V. Barth, *J. Am. Chem. Soc.* **2008**, *130*, 11778–11782.
[12] T. J. Lawton, J. Carrasco, A. E. Baber, A. Michaelides, E. C. H. Sykes, *Phys. Rev. Lett.* **2011**, *107*, 256101.
[13] F. Vidal, E. Delvigne, S. Stepanow, N. Lin, J. V. Barth, K. Kern, *J. Am. Chem. Soc.* **2005**, *127*, 10101–10106.
[14] A. Kühnle, T. R. Linderoth, B. Hammer, F. Besenbacher, *Nature* **2002**, *415*, 891–893.
[15] W. Xu, R. E. A. Kelly, H. Gersen, E. Lægsgaard, I. Stensgaard, L. N. Kantorovich, F. Besenbacher, *Small* **2009**, *5*, 1952–1956.
[16] P. Messina, A. Dmitriev, N. Lin, H. Spillmann, M. Abel, J. V. Barth, K. Kern, *J. Am. Chem. Soc.* **2002**, *124*, 14000–14001.
[17] H. Kong, L. Wang, Q. Sun, C. Zhang, Q. Tan, W. Xu, *Angew. Chem. Int. Ed.* **2015**, *54*, 6526–6530; *Angew. Chem.* **2015**, *127*, 6626–6630.

[18] K. L. Svane, M. S. Baviloliaei, B. Hammer, L. Diekhöner, *J. Chem. Phys.* **2018**, *149*, 164710.
[19] N. Abdurakhmanova, A. Floris, T.-C. Tseng, A. Comisso, S. Stepanow, A. De Vita, K. Kern, *Nat. Commun.* **2012**, *3*, 940.
[20] H. Kong, L. Wang, Q. Tan, C. Zhang, Q. Sun, W. Xu, *Chem. Commun.* **2014**, *50*, 3242 – 3244.
[21] P. Han, K. Akagi, F. Federici Canova, H. Mutoh, S. Shiraki, K. Iwaya, P. S. Weiss, N. Asao, T. Hitosugi, *ACS Nano* **2014**, *8*, 9181 – 9187.
[22] B. Yang, N. Cao, H. Ju, H. Lin, Y. Li, H. Ding, J. Ding, J. Zhang, C. Peng, H. Zhang, J. Zhu, Q. Li, L. Chi, *J. Am. Chem. Soc.* **2019**, *141*, 168 – 174.
[23] M. Böhringer, K. Morgenstern, W.-D. Schneider, R. Berndt, *Angew. Chem. Int. Ed.* **1999**, *38*, 821 – 823; *Angew. Chem.* **1999**, *111*, 832 – 834.
[24] Q. Li, C. Han, S. R. Horton, M. Fuentes-Cabrera, B. G. Sumpter, W. Lu, J. Bernholc, P. Maksymovych, M. Pan, *ACS Nano* **2012**, *6*, 566 – 572.
[25] A. D. Jewell, S. M. Simpson, A. Enders, E. Zurek, E. C. H. Sykes, *J. Phys. Chem. Lett.* **2012**, *3*, 2069 – 2075.
[26] Z. H. Cheng, L. Gao, Z. T. Deng, N. Jiang, Q. Liu, D. X. Shi, S. X. Du, H. M. Guo, H. J. Gao, *J. Phys. Chem. C* **2007**, *111*, 9240 – 9244.
[27] M. Böhringer, K. Morgenstern, W.-D. Schneider, R. Berndt, F. Mauri, A. De Vita, R. Car, *Phys. Rev. Lett.* **1999**, *83*, 324 – 327.
[28] S. Gottardi, K. Muller, J. C. Moreno-Lopez, H. Yildirim, U. Meinhardt, M. Kivala, A. Kara, M. Stohr, *Adv. Mater. Interfaces* **2014**, *1*, 1300025.
[29] T. Yokoyama, T. Takahashi, K. Shinozaki, M. Okamoto, *Phys. Rev. Lett.* **2007**, *98*, 206102.
[30] P. Maksymovych, J. T. Yates, Jr., *J. Am. Chem. Soc.* **2008**, *130*, 7518 – 7519.
[31] P. Maksymovych, D. C. Sorescu, K. D. Jordan, J. T. Yates, Jr., *Science* **2008**, *322*, 1664 – 1667.
[32] P. Tegeder, *J. Phys. Condens. Matter* **2012**, *24*, 394001.

Manuscript received: July 30, 2019
Revised manuscript received: August 21, 2019
Accepted manuscript online: September 18, 2019
Version of record online: November 19, 2019

